Multi-decadal simulation of estuarine sedimentation under sea level rise with a response-surface surrogate model

Matthew W. Brand[a,*], Leicheng Guo[b], Eric D. Stein[c] and Brett F. Sanders[a,d]

[a] Department of Civil and Environmental Engineering, Calit2 Building, University of California, Irvine, Irvine, CA 92617
[b] State Key Lab of Estuarine and Coastal Research, East China Normal University, Shanghai 200241, China
[c] Southern California Coastal Water Research Project, Costa Mesa, CA 92626, USA
[d] Department of Urban Planning and Public Policy, University of California, Irvine, Irvine, CA 92617, USA

ARTICLE INFO

Keywords:
sedimentation
hydromorphodynamic modelling
Delft3D
sea-level rise
surrogate modelling

ABSTRACT

Multi-decadal prediction of estuarine sedimentation with high-fidelity hydromorphodynamic models presents high computation costs, especially when accounting for stochasticity and uncertainty. A StochAstic model for Multi-decadaL Estuarine Sedimentation (SeAMLESS) is formulated here to support a specific decision-need related to resilience planning and coastal management: estimating future sedimentation and dredging within a sedimentation basin for different scenarios of sea level rise and rules for dredging. SeAMLESS combines a reduced-dimension process model and a response-surface surrogate model to yield an ordinary differential equation that can be integrated over stochastic time series of storm events. Applications show that SeAMLESS can predict probabilities and amounts of future basin sedimentation and dredging with minimal loss of accuracy, compared to a high-fidelity model, while delivering $\mathcal{O}(10^4 - 10^5)$ reduction in computational costs.

1. Introduction

Estuaries are embayments open to coastal oceans that receive freshwater runoff (Pritchard, 1967), and are increasingly confronted by climate change and the effects of urban development around the embayment and/or in the watershed such as land reclamation and waste discharges (Lotze et al., 2006). Estuaries represent critical coastal habitats that support ecosystems including birds, fish and invertebrates (McLusky and Elliott, 2004). Additionally, estuaries provide benefits to society (or ecosystem services) including recreational opportunities for coastal communities, pollutant and nutrient processing, support for the shipping, defense and fishing industries, and urban amenities such as access to wildlife, seafood, and open spaces (Barbier et al., 2011). These many benefits are often in competition and need to be balanced, thus posing challenges for management (Elliott and Whitfield, 2011).

Excess sedimentation is one of the costliest and potentially environmentally damaging management challenges of estuaries (Chesapeake Bay Program, 2006; Kiefer et al., 2000). Excess deposition negatively affects navigation and damages ecosystems by submerging wetland habitat and changing inundation regimes. Changes to bathymetry can negatively affect circulation and water quality, and the introduction of non-native or invasive species through dredging operations can reduce or degrade habitat for sensitive marsh animals (Haltiner et al., 1996). Management options such as source control and dredging are costly. Dredging requirements from federal, state and local agencies in the

mbrand1@uci.edu (M.W. Brand)
ORCID(s):

United States are expected to reach $2 billion/year, with the U.S. Army Corps of Engineers spending $1.3 billion in 2015 alone (US Army Corps of Engineers et al., 2016). Moreover, predicting future dredging requirements is difficult due to uncertain variability in estuarine dynamics and inherent complexities in sedimentation, watershed and tidal dynamics and significant changes due to human influences (Bull et al., 2002). In particular, estuarine sedimentation is driven by watershed runoff and tidal currents which vary with hourly and longer time scales and are also affected by sea level rise (SLR) and land-use/management changes (McLusky and Elliott, 2004; Griggs et al., 2017). High-fidelity deterministic models such as Delft3D are oftentimes used to answer questions on estuarine sedimentation (Yu et al., 2012; Thanh et al., 2019). Arid regions such as southern California experience highly episodic hydrology with stream flows that vary by several orders of magnitude over time scales of hours to a few days. Here, greater than 90% of sedimentation occurs quickly during the most intense storms (Kroll, 1975; Warrick and Milliman, 2003). The wide range of variability in process magnitude and time scales, along with significant uncertainty in model input parameters, makes it virtually impossible to deterministically predict future sedimentation and associated dredging requirements, thereby motivating the need for stochastic modeling approaches.

Stochastic modeling, notably with Monte Carlo simulations, has increasingly been used in environmental studies to characterize ranges and likelihoods of system outcomes over time scales of days, months, years and even decades or centuries (Fedra, 1983). Furthermore, stochastic modeling is especially useful for environmental management because probabilities are assigned to a range of outcomes, creating opportunities to enhance dialogue and deliberation among stakeholders towards development of cost effective and fair management measures (Isukapalli et al., 1998). However, a major limitation of stochastic modeling stems from complex, interdependent, environmental process dynamics that require use of mechanistic models with high computational demands (Sparrevik et al., 2012), or so-called *high-fidelity models*. Use of high-fidelity models make it very difficult or even impossible to complete the thousands or more Monte Carlo simulations needed to account for stochasticity (Liu et al., 2007).

Fast-running surrogate models have emerged as a promising alternative to high-fidelity models with demonstrated ability to radically reduce computational costs (Razavi et al., 2012). One type of surrogate model is a response-surface function, which captures relationships (e.g., through polynomial approximations) between several explanatory variables of a system (Razavi et al., 2012; Koziel and Leifsson, 2013). These response surfaces are developed by running a relatively modest number of high-fidelity model simulations over a carefully selected set of input parameter values (Razavi et al., 2012; Koziel and Leifsson, 2013). Once the surrogate model is trained to quantify the desired system outcomes over a suitable parameter space, thousands or even millions of Monte Carlo simulations can easily be completed with significantly reduced runtimes compared to the mechanistic model (Fedra, 1983; Isukapalli et al., 1998; Liu et al., 2007; Razavi et al., 2012; Koziel and Leifsson, 2013). Examples of response surface surrogate models in water resources include optimization studies (Razavi et al., 2012), improving aquifer management and regulatory support

(Schultz et al., 2004; Sreekanth and Datta, 2011; Kourakos and Mantoglou, 2009), and model selection (Mohammadi et al., 2018). Another type of surrogate model is a lower fidelity model, which can be viewed as a lower-resolution versions of a high resolution model (Razavi et al., 2012).

Within the field of sediment transport and hydromorphodynamics, Berends et al. (2019) present a low fidelity surrogate modeling approach for characterizing the uncertainty of estuarine sedimentation predicted by a high-fidelity model. The lower resolution model reduced run times by a factor of sixteen compared to the high fidelity model (or 6.25%), which allowed for an 85% reduction in the overall compute time needed to map out sedimentation patterns (and uncertainties) using a Monte Carlo approach. Additionally, Mohammadi et al. (2018) describe a response surface surrogate model for a hydro-morphodynamic model (TELEMAC-MASCARET with SISYPHE module) of the lower Rhine river where Bayesian model selection is applied to discern the best choice among empirical sediment transport equations. Here, the response surface surrogate model was applied to quantify the sedimentation uncertainty and model dependence on uncertain parameters. Nevertheless, use of surrogate modeling within hydro-morphodynamic simulation is relatively new.

In this paper, we present a new approach to simulate estuarine sedimentation and rule-based dredging over multiple decades by combining a reduced-dimension process model and a response surface surrogate model within a stochastic Monte Carlo simulation framework. We term this framework the StochAstic model for Multi-decadaL Estuarine Sedimentation (SeAMLESS). The proposed framework is a response to the engagement of coastal stakeholders in southern California under the SedRISE project (Resilient Infrastructure and Sustainable Environments) funded by the Ecological Effects of Sea Level Rise Program (EESLR) of the National Centers for Coastal Ocean Science at the National Oceanic and Atmospheric Administration. The EESLR program supports transdisciplinary research projects where stakeholders are engaged with the aim of closing the “usability gap" between what scientists and decision-makers consider useful climate-rated knowledge (DeLorme et al., 2016).

In southern California and elsewhere, there is a need to plan for accelerating rates of sea level rise and consider changes to sediment management to yield outcomes favorable to coastal ecosystems, flood risk management, and financial stewardship (Passeri et al., 2015; Morris et al., 2016; Bilskie et al., 2016). Sea level rise threatens submergence of coastal wetlands (Thorne et al., 2018) and increased flood risk (Gallien et al., 2011; Sanders et al., 2020), yet the amounts of sea level rise is highly uncertain and partial mitigation of these impacts may be possible through altered sediment management practices (Sanders and Grant, 2020; Ulibarri et al., 2020).

The remainder of the paper is organized as follows: Section 2 presents the theoretical formulation of SeAMLESS including the development of a reduced-dimension process model that can be integrated efficiently with the aid of a response-surface surrogate model. Section 3 presents an application of SeAMLESS to a site in southern California, Newport Bay, where sediment fluxes have been subject to management since the 1980s and there is a need to consider sea level rise in adaptation and resilience planning. Section 4 continues with a second application of SeAMLESS to a larger, stylized, system for which a high-fidelity model can more easily be run over long time scales. This affords a more critical examination of the SeAMLESS framework based on side-by-side comparisons of SeAMLESS and high-fidelity model simulations for the same series of storm events. Section 5 closes the paper with conclusions.

2. SeAMLESS Formulation

2.1. Decision-Support with High-Fidelity Process Models

High-fidelity models for hydro-morphodynamics such as Delft3D (Lesser et al., 2004) numerically solve process-based equations describing fluid flow, sediment transport and movement of the fluid/bed interface at fine spatial and temporal scales (Lesser et al., 2004). The solution state of a hydro-morphodynamic model can be defined by $\mathbf{U}(\mathbf{x}, t)$ where $\mathbf{x} \in \mathbf{R}^3$ represents the spatial dimensions, t, represents time, and elements of $\mathbf{U}$ include the fluid velocity $\mathbf{u}$, ground elevation z_b, sediment concentrations c_i for a set of i grain sizes, fluid pressure p, and fluid density ρ. A general representation of hydro-morphodynamic models is a system of partial differential equations for $\mathbf{U}(\mathbf{x}, t)$ that is solved on a spatial domain $\mathcal{D}$ and time interval $t = (0, T)$ as follows,

$$\frac{\partial \mathbf{U}}{\partial t} = \mathbf{M}_U(\mathbf{U}, \mathbf{I}) \tag{1}$$

where $\mathbf{M}_U$ is an operator representative of the hydro-morphodynamic simulation model, and $\mathbf{I}$ contains the model inputs that influence the solution, including initial conditions, boundary conditions and model parameters. Once the solution is simulated, additional operations follow to produce information that is used for decision-making. That is, decision-makers likely won't want to know the spatial distributions of fluid velocity, pressure, and density, but rather some integral measures reflective of the level of sedimentation in the system (total volume of sediment) and/or the overall water quality of the system. Hence, there exists a set of decision variables $\mathbf{D}$ that are obtained by operating on the solution state ($\mathbf{M}_D$) as follows,

$$\mathbf{D} = \mathbf{M}_D(\mathbf{U}) \tag{2}$$

Decision variables need to be relatively simple, and hence $\mathbf{D}$ will generally contain orders of magnitude fewer scalar elements than $\mathbf{U}$, and maybe even just one or two, such as the maximum height of the sediment bed within a collection basin or the total volume of sediment in collection basin. Generally, to meet decision-support needs with high-fidelity models, numerous (computationally demanding) simulations are run (Eq. 1) to generate output describing the spatial and temporal evolution of the solution state, and then results are post-processed (Eq. 2) to distill decision variables as shown in Fig. 1a.

2.2. Reduced Dimension Process Model and Surrogate Model

A common decision variable is the spatially averaged value of a system property, $\overline{\mathbf{U}}(t)$, taken over a subset of the model domain, $\mathcal{D}_D \subset \mathcal{D}$. The subdomain $\mathcal{D}_D$ is chosen to align with the decision-making needs, and in the case of estuarine sedimentation, aligns with the spatial extent of a regulatory sedimentation zone (or basin) where dredging is permitted to occur. A general representation of the time-wise changes of the spatially-averaged solution state within the regulatory basin is given by the following ordinary differential equations (ode) that is solved for the time interval $t = (0, T)$,

$$\frac{d\overline{\mathbf{U}}}{dt} = \overline{\mathbf{M}}_U(\overline{\mathbf{U}}, \mathbf{I}) \tag{3}$$

where the operator $\overline{\mathbf{M}}_U$ represents the bulk effects of hydromorphodynamic processes over the spatial extent of subdomain $\mathcal{D}_D$. In the case of sedimentation and dredging, the key decision-variable is simply the total volume of sediment that has accumulated in a regulatory sedimentation basin, thus Eq. 3 simplifies as follows,

$$\frac{d\overline{z_\mathrm{b}}}{dt} = \overline{\mathbf{M}}_z(\overline{\mathbf{U}}, \mathbf{I}) \tag{4}$$

where $\overline{\mathbf{M}}_z$ is a refinement of $\overline{\mathbf{M}}_U$ that supports output of a single scalar describing the rate of change in average bed elevation as a function of the system state and inputs. It is possible to analytically derive the operator $\overline{\mathbf{M}}_z$ from the operator $\mathbf{M}_U$ and the subdomain $\mathcal{D}_D$, discretize the resulting process-based terms, and numerically integrate the solution to yield predictions of $\overline{z_\mathrm{b}}(t)$. However, this process-based approach is not pursued herein. Rather, we introduce a data-driven approach using a response surface surrogate model, $\tilde{\mathbf{M}}_z$, as follows,

$$\frac{d\overline{z_\mathrm{b}}}{dt} = \tilde{\mathbf{M}}_z(\overline{\mathbf{U}}, \mathbf{I}) \tag{5}$$

whereby the surrogate model depicts the time rate of change of the basin-average sediment bed height based on model inputs and system conditions that are found, through a diagnostic process, to represent the primary controls. Furthermore, the response surface surrogate model is quantified by solving the high-fidelity model over a representative range of the control variables, which essentially organizes a database or library of known responses that can be accessed as needed to numerically integrate Eq 5. Hence, by combining a reduced-dimension process model and a response surface surrogate model, decision-support needs can be met by numerically integrating an ordinary differential equation (Eq. 5) while leveraging data produced by a high-fidelity model as shown in Fig. 1b.

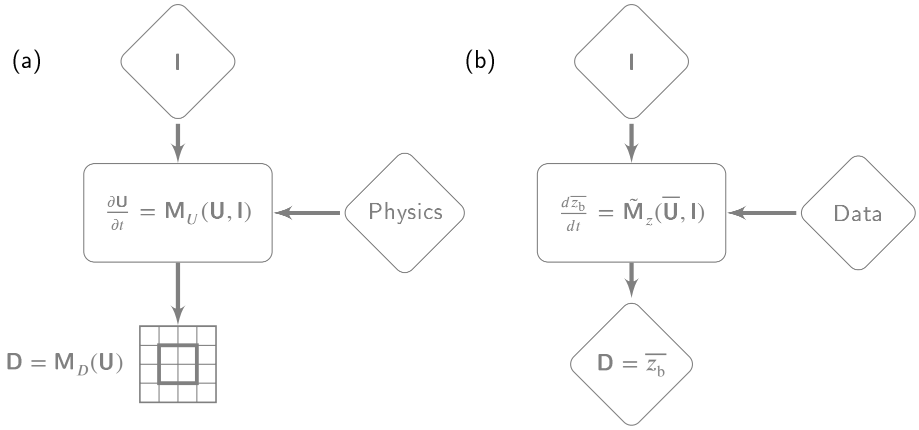

Figure 1: Estimation of decision-support variables, **D**, using: (a) high-fidelity method involving numerical solution of partial differential equations based on flow physics and post-processing of gridded model output and (b) proposed reduced-dimension, response-surface surrogate modeling approach that uses "Data" generated by a high-fidelity model.

Site-specific considerations will influence the design of the response-surface surrogate model, $\tilde{\mathbf{M}}_z$ Eq. 5, such as the size of the estuary, the configuration of the sedimentation basin, the tidal dynamics of the estuary, and the magnitude and variability of streamflow into the estuary. In southern California, there are many tidally-influenced lagoons, flood control channels, harbors and embayments subject to sedimentation and dredging. These systems are characterized by relatively short lengths and negligible tidal amplification. Tides in the region have micro-tidal amplitudes (~ 1 m) with temporal asymmetry that favors export of coarse and fine sediment to the coastal ocean, although in some systems, tidal asymmetry may favor the import of coarse or fine sediment (Guo et al., 2018; Nidzieko, 2010). Additionally, inputs of streamflow and sediment are highly episodic. Sediment loads vary by orders of magnitude with storm events (Warrick and Milliman, 2003), which last less than a day, and more than 90% of sedimentation occurs during the most intense storms (Kroll, 1975; Warrick and Milliman, 2003). Combining mass balance considerations and sub-daily time scale of storm events, we can re-formulate Eq. 5 as follows,

$$\frac{d\overline{z_b}}{dt} = \frac{1}{\rho_s A}\frac{dm}{dt} \tag{6}$$

where m and A are the sediment mass and planform area of the sedimentation basin, respectively and ρ_s is the dry bed density of the sediment. Furthermore, we can integrate over the time scale of a storm event, T, to yield an equation for event-based change in sediment basin elevation as follows,

$$\Delta\overline{z_b} = \int_t^{t+T} \left(\frac{d\overline{z_b}}{dt}\right) dt = \frac{\Delta m}{\rho_s A} \tag{7}$$

and thus we can advance the sediment basin elevation in time from t_i to t_{i+1} as follows,

$$(\overline{z_\mathrm{b}})_{i+1} = (\overline{z_\mathrm{b}})_i + \frac{\Delta m_i}{\rho_\mathrm{s} A} \tag{8}$$

subject to an initial condition $(z_\mathrm{b})_0$ at time t_0 which focuses attention on the need for a surrogate model that characterizes the event-based deposition of mass within the sediment basin, Δm_i. Taking the event-based watershed load of sediment to be L_i, we can write the event based deposition as,

$$\Delta m_i = \eta_i L_i \tag{9}$$

where η represents the capture efficiency of the sedimentation basin, i.e., the fraction of the sediment load from a storm event that is deposited in the basin. Moreover, through a sensitivity analysis using a high-fidelity model (described in the following section), we find that the primary factors affecting the capture efficiency of the sediment basin are the peak discharge of the storm event, Q, the average basin elevation $\overline{z_\mathrm{b}}$, and the tidal conditions (which we denote as ϕ). Hence, event-based changes in sediment mass required to update Eq. 8 are computed using a response surface surrogate model for capture efficiency, $\tilde{\eta}$, as follows,

$$\Delta m_i = \tilde{\eta}\left(Q_i, (\overline{z_\mathrm{b}})_i, \phi_i\right)\ L_i \tag{10}$$

which points to the need for high-fidelity model simulations over a parameter space defined by ranges in Q, $\overline{z_\mathrm{b}}$, and ϕ_i to create a library of solutions from which values of η can be estimated by interpolation as (e.g., Razavi et al., 2012). Further detail on surrogate model parameterization is left for the next section, which presents an application of SeAMLESS to a site in southern California.

Two final factors must be considered to support multi-decadal simulations of sedimentation: sea level rise and dredging events. The former is approached by assuming that the height of the sediment bed is measured with respect to a tidal datum, mean sea level, which implies that increases in mean sea level correspond to decreases in the bed elevation. Secondly, dredging events are modeled by assuming that removal of sediment occurs when the sediment bed elevation reaches a trigger point, $(\overline{z_\mathrm{b}})_\mathrm{trig}$, and that the sediment bed elevation is lowered to the initial height $(\overline{z_\mathrm{b}})_0$. Moreover, we assume that the post-dredging sediment height and trigger height are also measured relative to a tidal datum, which preserves the range of depths that occur in the sedimentation basin as sea level rises. Combining Eqs. 8

and 10, the final update equation is given as follows,

$$\left(\overline{z_{\mathrm{b}}}\right)_{i+1}=\begin{cases}\left(\overline{z_{\mathrm{b}}}\right)_{i}+\tilde{\eta}\left(Q_{i},(\overline{z_{\mathrm{b}}})_{i},\phi_{i}\right)\frac{L_{i}}{\rho_{\mathrm{s}}A}-\left(\Delta z_{\mathrm{SLR}}\right)_{i}, & \text{if } \overline{z_{\mathrm{b}}}\leq(\overline{z_{\mathrm{b}}})_{\mathrm{trig}}\\ \left(\overline{z_{\mathrm{b}}}\right)_{0}, & \text{if } \overline{z_{\mathrm{b}}}>(\overline{z_{\mathrm{b}}})_{\mathrm{trig}}\end{cases}\tag{11}$$

subject to the initial condition given by $(\overline{z_{\mathrm{b}}})_0$, and where $\left(\Delta z_{\mathrm{SLR}}\right)_i$ represents the change in (absolute) sea level between t_i and t_{i+1}. Note that increases in sea level rise act against the effect of sedimentation. Hence, as rates of sea level rise increase, the amount of sedimentation required to trigger a dredging event increases. Moreover, in the event that the rate of sea level rise is faster than the rate of sedimentation, it is not possible for the sediment bed elevation to reach the trigger height and thus no dredging events occur.

The SeAMLESS framework described herein represents a significant departure from previous sedimentation modeling frameworks involving surrogate modeling (e.g., Mohammadi et al., 2018; Berends et al., 2019). Whereas previous work focused on more efficiency estimation of uncertainty in sedimentation (Berends et al., 2019) and improved selection of empirical equations for sediment transport rates (Mohammadi et al., 2018), herein we use a response surface surrogate model to evaluate the right hand side of reduced dimension model described by an ordinary differential equation, which in turn is configured to account for human influences on sedimentation (dredging events) as well as changes in mean sea level due to sea level rise. With this approach, the SeAMLESS framework is positioned to make multi-decadal predictions of sedimentation and dredging under different sea level rise scenarios and dredging rules, which is responsive to coastal management decision-making needs in southern California and elsewhere.

2.3. Surrogate Model Construction Process

Constructing the response surface surrogate model will rely upon modeling expertise coupled with an iterative process to identify key model sensitivities. It is highly unlikely that two surrogate models constructed for different regions will ever look the same, or even that key state variable and parameters will remain constant. The general overview of model construction is provided to the reader below in list format.

1. Develop, calibrate, and validate high-fidelity hydromorphodynamic model using best available data,
2. Identify basin with a well-defined geographic boundary and major controls on basin elevation,
3. Utilize high-fidelity model to explore parameter and state variable space to identify key model sensitivities (flow, tidal condition, sediment characteristics, dredging, basin elevation) with which to construct response surface surrogate model,
4. Compare the surrogate model to high fidelity model output and measured basin elevations to evaluate model performance,

5. Utilize Monte-Carlo or Monte-Carlo Markov Chain model to simulate forcing data and use surrogate model to predict future basin elevations.

3. SeAMLESS Application to Newport Bay

3.1. Site Description

SeAMLESS is applied to Newport Bay, a short (10km) estuary in southern California that receives sediment input primarily from San Diego Creek (SDC, shaded blue), as shown in Figure 2. The upper portion of the bay contains protected wetland habitat while the lower portion is used as a recreational harbor. Historically, excessive sedimentation from SDC was the greatest driver of habitat change in Newport Bay, threatening to turn protected wetlands into upland habitat (Trimble, 1997). As a result, a sediment management strategy for a total maximum daily load (TMDL) for SDC was implemented, stipulating a 50% reduction in overall sediment loads in addition to maintaining a minimum depth of 2.13 meters below MSL for subtidal habitat in Upper Newport Bay (UNB) (Board, 2014). Newport Bay contains two sediment capture basins (outlined in red, Figure 2), Basin I/III at the mouth of SDC and Basin II, further downstream of SDC, constructed in 2010 at a cost of $37 million dollars as part of the sediment TMDL with estimated lifespans of 20 years (USACOE, 2011). Hydrodynamic calibration was reported by Guo et al. (2018) and additional calibration and evaluation for sedimentation appears in the Section 3.5.

Sedimentation (and the corresponding elevation) of the UNB sediment capture basins is driven by both natural processes and human influences. Natural processes include fluvial input and transport by estuarine currents, which are primarily affected by streamflow and tidal changes in ocean water levels at the mouth of the estuary. Human influences include land uses that affect runoff and the upstream sources of sediment, flood control infrastructure which affects the rate and intensity of streamflow and sediment loads, and dredging which affects tidal circulation. Moreover, human influences are shaped by watershed and estuarine management policies including the sediment TDML and dredging policy. Presently, dredging is required when the sediment capture basins fill to an elevation of 2.13 m below MSL. When that "trigger point" is reached, sediment is dredged to the original basin elevation of 6.65 m below MSL and disposed of offshore, removing them from the system permanently (Board, 2014; USACOE, 2011). Hence, $(\overline{z_b})_{\mathrm{trig}}$= -2.13 m and $(\overline{z_b})_0$= -6.65 m.

3.2. Hydrologic, Oceanographic, and Bathymetric Data

Stream flow and sediment loading data were acquired for SDC at Campus Drive, a short distance upstream of the connection to Newport Bay. This included a 25–year record of daily peak flow (Figure S10) and a concurrent five-year year record of five-minute interval instantaneous flow data (Figure S1). Sediment transport curves as a function of flow for the same time period were provided by OC Public Works Sediment TMDL Reports ((County of Orange,

Figure 2: Newport Bay is an urban estuary of southern California where sediment is managed for water quality, wetland habitat, recreation, navigation and the provision of urban amenities. Dredging focuses on sediment capture basins (Basin II and Basin I/III) and a TMDL was implemented to regulate watershed loads from San Diego Creek (highlighted in blue).

2016), Figure S2). Oceanic water level measurements for the period of interest are available from the Los Angeles tide gage (NOAA Gage 9410660). Bathymetric data of UNB for the years 2011, 2012, 2013 and 2015 at 2.1 meter horizontal resolution (vertical errors not reported) were available as a result of TMDL compliance monitoring by the Army Corps of Engineers, and dredging excavation depths were available for 2010 (USACOE, 2011). A 2014 survey of Lower Newport Bay (LNB) bathymetry at 7.6 meter horizontal resolution (vertical accuracy of 15 cm) was used for LNB (USACE, personal communication), and the 2013 NOAA Coastal Topobathy was used to model land elevation and offshore bathymetry (horizontal resolution of 1 meter, land vertical accuracy of 4.8 cm RSME, offshore bathymetry vertical accuracy of 15 cm RSME) (Dewberry, 2013).

Table 1
Model parameters, units, ranges used in sensitivity analysis, and final calibrated value.

Model Parameter	Units	Range	Final Calibrated Value
Chezy Bottom Roughness Coefficient	$\frac{m^{1/2}}{s}$	0 - 1,000	65
Sand Dry Bed Density	$\frac{kg}{m^3}$	1,300 - 2,100	1,600
Mud Dry Bed Density	$\frac{kg}{m^3}$	300 - 500	350
Sand D_{50}	m	Default Value	1×10^{-4}
Critical Stress for Erosion	$\frac{N}{m^2}$	0.16 - 0.75	0.16
Critical Stress for Sedimentation	$\frac{N}{m^2}$	0.1 - 1,000	0.11
Mud Settling Velocity	$\frac{m}{s}$	Default Value	0.00025
Maximum Mud Concentration	$\frac{kg}{m^3}$	10 - 15	12

3.3. High-Fidelity Model: Delft3D

A two-dimensional (depth-integrated) Delft3D model (version 4.01.01) was constructed with a domain including the lower part of the San Diego Creek, Newport Bay and a nearshore zone. Delft3D resolves fluid flow, sediment transport, and morphodynamics at fine spatial and temporal scales and has received widespread use for coastal hydromorphodynamics (Lesser et al., 2004). Delft3D was configured with an inland inflow boundary where the instantaneous volumetric flow rate and sediment load is specified, and an open boundary around 8 km offshore where water level is specified. The model mesh contains approximately 46,519 cells with high resolution in the bay and a minimum cell size of 5×10 m, with lower resolution offshore and a maximum cell size of roughly 150×350 m. The computational mesh and flow resistance parameters are based on a hydrodynamic calibration and evaluation described in Guo et al. (2018). Bed erosion parameters in the Delft3D model were developed from field measurements and computational experiments (Stein, 2014). Delft3D was calibrated to match morphological change between 2011 and 2012, and then evaluated for the period 2010-2015. Five-minute interval flow data for 2010 to 2015 was used to specify the freshwater inflow from SDC (and sediment loading based on sediment transport curves) and six-minute interval tide measurements from Los Angeles were used to specify the water level at the offshore open boundary of the model. Calibration involved the manual adjustment of several parameters including the sediment curve, erosion/sedimentation thresholds, and dry density of mud within physically plausible ranges, which are shown in Table 1.

A morphological acceleration factor is usually used to achieve decadal to centennial morphodynamic changes (Roelvink, 2006), but for Newport Bay, spatially distributed bed levels were updated at each hydrodynamic time step (= 0.05 min) which corresponds to a morphological acceleration factor of unity. A sensitivity analysis using the highest tidal ranges (spring tide in January) and lowest erosion parameters measured in the bay (threshold for erosion $= 0.16$ N/m^2) found that little to no morphological changes occurred throughout the whole estuarine system during dry weather (< 1% of yearly morphodynamic change). Based on this analysis, dry weather events river discharge (< 20 cms) were ignored for the calibration and evaluation phases of the Delft3D modeling, and time integration of the Delft

Table 2
Measurements of sediment bed height and 2D and 3D Delft3D model predictions for a one year period, 2010-2011.

Unit I/III Basin Heights			
Year	Measured Height	Modeled Height (2D)	Modeled Height (3D)
2010	-6.654	-6.654	-6.654
2011	-6.294	-6.297	-6.109

Unit II Basin Heights			
Year	Measured Height	Modeled Height (2D)	Modeled Height (3D)
2010	-6.654	-6.654	-6.654
2011	-6.405	-6.333	-6.343

3D model was limited to the periods of time when SDC streamflow exceeded 20 cms. The tidal water level from the LA tide gauge was used for each storm to drive the oceanic boundary condition, with a period between storms driven by a tidal cycle of 9 to 57 hours. This was done to ensure that the previous storm was not impacting the hydrodynamics of the proceeding storm.

Two sediment fractions, one non-cohesive sand (grain size of 100 μm) and one cohesive mud (settling velocity of 0.25 mm/s), were used to simulate sediment transport, erosion and deposition. The largest source of sediment in this system is fine material from San Diego Creek. Data collected as part of sediment TMDL found that fines constitute approximately 56-96% of the total load in San Diego Creek, model calibration found that a 95% mud fraction yielded the closest agreement between model and data (County of Orange, 2016, 2013). The concentrations of fines are defined by the sediment rating curves (see Fig. S2) based on 25 years of flow and sediment measurements by OC public works (County of Orange, 2016). The relatively small sand fraction of the sediment load is modeled under the assumption of equilibrium concentrations and an unlimited supply of available sediment (Van Rijn et al., 1993; Deltares, 2014).

The dry bed densities are 1,600 kg/m^3 and 350 kg/m^3 for sand and mud, respectively. The Van Rijn et al. (1993) formula is employed to calculate non-cohesive sand transport in which both bed load transport and suspended sediment transport are taken into account. Details of the Van Rijn et al. (1993) formulae can be found in the user manual of Delft3D (Deltares, 2014) and Van Rijn et al. (1993) thus are not repeated here. For cohesive sediment, the Partheniades-Krone formulation is applied to calculate mud transport (Partheniades, 1965). The critical erosion of the mud used were set to measured values and are 0.16 N/m^2 (Stein, 2014). The critical threshold for deposition was calibrated to 0.11 N/m^2 from 1,000 N/m^2 (which resulted in a calibration basin height of -6.14 m for the year 2012 compared to -6.04 m when using 0.11 N/m^2 and a measured value of -6.047), for the Unit I/III basin. These values suggest that erosion only happens when the calculated bed shear stress is $>$0.16 N/m^2 and deposition occurs when shear stress is $<$0.11 N/m^2 (Deltares, 2014; RMA, 1998).

A two-dimensional approach was used over a three-dimensional formulation (using 10-σ layers) based on the results of a 2D vs. 3D comparison for a one year period, 2010-2011. As shown in Table 2, the 2D model performed better than the 3D model in the Unit I/III basin, with a 3 mm difference in modeled vs measured average basin elevation compared to the 3D model's 18 cm difference. In the Unit II basin, the 3D model performed slightly better than the 2D model, with only a 1 cm difference between the two. Unit I/III basin is largely well mixed (Trimble, 2003), so the 3D model introduces extra physical processes which increases potential model uncertainty and noise, explaining the differences between the 2D and 3D model. Other studies have found that a 2D works equivilently well compared to 3D approach for hydrodynamics /salinity (Sandbach et al., 2018) and sediment transport modeling in estuarine systems (Achete et al., 2017) Based on the lack of improvement in model accuracy, and very significant gains in computational speed (roughly 10 times faster), the 2D Delft3D model was chosen to finish model evaluation and develop the surrogate model.

3.4. Response Surface Surrogate Model

The surrogate model can only be built after a numeric model (such as Delft3D) is calibrated and evaluated, at which point numeric model parameters are not changed. Then, the surrogate model can be constructed and evaluated against measured data to ensure surrogate model robustness. To develop the response surface surrogate model, the high fidelity model was configured to simulate 24 hour storm events based on the peak flow into the estuary, Q, a triangular hydrograph shape with a 5 hour and 11 hour time to rise and fall, respectively, a pre-event sediment basin elevation, $\overline{z}_\mathrm{b}$, and a mixed regime tidal boundary (to match the tides at Newport Bay) with a period of 13.3 hours, an amplitude, a, and a phase ϕ. These results showed that the most important variables to consider for estimating the sediment capture efficiency, $\tilde{\eta}$, are the flood peak and the pre-event basin elevation. Furthermore, results showed that the phasing and amplitude of the tide had a secondary effect, with the maximum deposition occurring when the flood peak occurred during the maximum flood currents of a spring tide and the minimum deposition occurring when the flood peak was timed with maximum ebb currents of a spring tide for this system. Capturing all possible combinations of tidal amplitude and phase would introduce two additional independent variables to the response surface surrogate model (in addition to Q and $\overline{z}_\mathrm{b}$), and assuming that m different values of each independent variable would need to be sampled to map out $\tilde{\eta}$, the required number of high-fidelity model runs would increase from m^2 to m^4, an increase by a factor m^2. This motivated the formulation of capture efficiency as a weighted average of the minimum and maximum capture efficiency over the tidal cycle, ($\tilde{\eta}_\mathrm{min}$ and $\tilde{\eta}_\mathrm{max}$, respectively) as follows,

$$\tilde{\eta}\left(Q, \overline{z}_\mathrm{b}, \phi\right) = [1-\theta] \times \tilde{\eta}_\mathrm{min}\left(Q, \overline{z}_\mathrm{b}\right) + \theta \times \tilde{\eta}_\mathrm{max}\left(Q, \overline{z}_\mathrm{b}\right) \tag{12}$$

where θ is a weighting factor that is treated as a random variable between zero and unity. In southern California, tidal amplitudes transition between small neap tides to large spring tides with a fortnightly cycle, and also experience

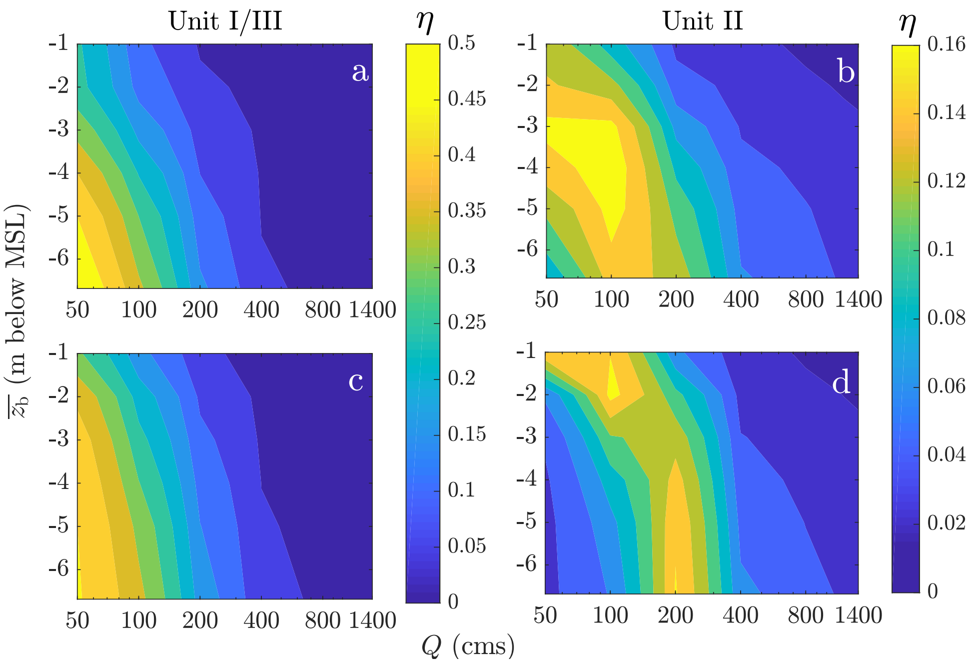

Figure 3: Response surface surrogate models $\tilde{\eta}_{\mathrm{ebb}}$ (a,b) and $\tilde{\eta}_{\mathrm{flood}}$ (c,d) for Basin I/III (a,c) and Basin II (b,d) of Newport Bay. Note that the x-axis is logarithmic and only shows storms from 50 cms to 1,400 cms for visual clarity.

semi-diurnal and diurnal variability. Where a flood peak falls within this cycle is, in fact, random. Hence, treating θ as a random variable in Eq. 12 with a uniform distribution between zero and unity leads to a surrogate model for sediment capture efficiency that accounts for both deterministic (Q and $\overline{z}_b$) and random (tidal conditions) aspects of the system. In the case of Newport Bay, the maximum capture efficiency was found to occur when the flood peak was coincident with the peak flood current ($\tilde{\eta}_{\mathrm{max}} = \tilde{\eta}_{\mathrm{flood}}$), and the minimum capture efficiency was found to occur when the flood peak was coincident with the maximum ebb current ($\tilde{\eta}_{\mathrm{min}} = \tilde{\eta}_{\mathrm{ebb}}$). However, we anticipate that this could vary from site to site which reiterates the site-specific nature of a response-surface surrogate model. Future studies could investigate a diversity of sites and develop potentially develop generalizations of basin response surface surrogate model sensitivities to tides, flows, sediment supply and basin elevations.

Fig. 3 presents the response surfaces for $\tilde{\eta}_{\mathrm{ebb}}$ and $\tilde{\eta}_{\mathrm{flood}}$, respectively, for both the Unit I/III and Unit II basins. Basin I/III has an average η of 12.3% and 13.8% and Unit II with an η of 10.1% and 11.1% for peak ebb and flood currents, respectively. Additionally, these surfaces show the nonlinear response of capture efficiency to Q and $\overline{z}_b$ characterized by local maxima and minima. Importantly, mapping out this dependence using the high fidelity model positions the reduced-dimension surrogate model to efficiently make multi-decadal simulations with a high level of computational efficiency in two separate basins within the same system.

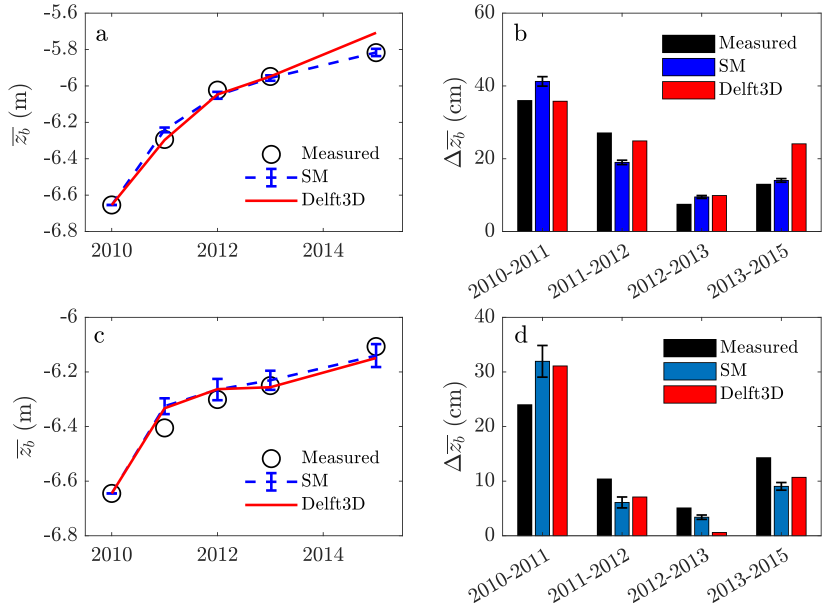

Figure 4: High-fidelity model (Delft3D) and SeAMLESS output (SM) compared to measured quantities of average basin elevation ($\overline{z_b}$, panels a & c) and yearly change in average basin elevation ($\Delta\overline{z_b}$, panels b & d) for the Unit I/III (panels a & b) and Unit II (panels c & d) basins. The error bars on the surrogate model account for model uncertainty due to tidal influence (θ), which is treated as a random variable.

3.5. SeAMLESS Evaluation

The high-fidelity model and SeAMLESS were both applied to simulate five years of sedimentation (30 storms exceeding baseflow threshold during 2010-2015) in Newport Bay which corresponds to a duration when annual bathymetric monitoring data are available for validation purposes and gauge measurements are available to specify model inputs including streamflow, sediment loads and tides. Figure 4 presents comparisons of the high-fidelity and reduced-dimension surrogate model predictions of $\overline{z}_b$ in Basin I/III and Basin II, which compare favorably to measured changes.

The models were quantitatively compared based on the Root Mean Square Error (RSME) in basin elevation. SeAMLESS performs better than the high-fidelity model for the Unit I/III basin ($\text{RSME}_{\text{Delft3D}}$ = 0.00253 m vs. RSME_{SM}=0.00072 m) and slightly worse for the Unit II basin ($\text{RSME}_{\text{Delft3D}}$=0.00166 m vs. RSME_{SM}=0.00180 m). This is likely due to stronger tidal currents in the Unit II basin which are also reflected by the larger error bars appearing in Figure 4c-d compared to Figure 4a-b. Furthermore, the SeAMLESS model uncertainty due to tidal influence bounds the high-fidelity model simulations for most years–the exception being years 2011 and 2015 in Unit I/III. The maximum yearly error (difference in deposition) was 0.081 m and 0.11 m for the surrogate and Delft3D models, respectively in the Unit I/III basin.

Relative runtimes of SeAMLESS and the high-fidelity model were examined with an 85 year simulation of Newport Bay. SeAMLESS was run using a single core on a 3.0 Ghz processor, while the high-fidelity model was run on a high-

Table 3
High-fidelity model runtimes and SeAMLESS speedup based on a runtime of 42 seconds.

System	Model Runtime (hrs)	SeAMLESS Speedup
1-core	6,033	5.16×10^5
4-core	3,448	2.95×10^5
8-core	1,675	1.43×10^5
16-core	1,370	1.17×10^5
32-core	944	8.07×10^4
64-core	359	3.07×10^4

performance computing cluster (64-core compute nodes with 2.33 GHz AMD processors and 512 GB of RAM) using 1 to 64 cores. We note that SeAMLESS integrates over flood events, and the high fidelity model integrates over periods with significant streamflow (not dry weather periods) although a short period (<24 hours) is modeled between wet-weather events for to allow the hydrodynamics to reset to a tidally forced state. SeAMLESS computes this simulation in 42 seconds, while the high-fidelity model run time varies from hundreds to thousands of hours depending on the number of cores. Table 3 presents the high-fidelity model runtimes and SeAMLESS speedup, defined by the ratio of the high-fidelity model runtime to the SeAMLESS runtime (for a single simulation). This shows that individual, multi-decadal simulations can be completed $\mathcal{O}(10^4 - 10^5)$ times faster using SeAMLESS without any obvious loss of accuracy in terms of basin-averaged decision variables of interest to stakeholders. Moreover, further gains in computational efficiency are possible through parallel execution of SeAMLESS simulations. These results show that SeAMLESS is ideally configured to support Monte Carlo Markov Chain simulations of sedimentation and dredging that account for a range of possible storm peak sequences, sea level rise trajectories, and dredging rules–modeling that would be prohibitively expensive using the high-fidelity model.

3.6. Multi-decadal SeAMLESS Simulation

Stochasticity is introduced to SeAMLESS for multi-decadal simulations with daily SDC peak flow (Q) based on a Monte-Carlo Markov Chain (MCMC) random sampling (see supplemental text for details on MCMC sampler, including historical data used to develop the sampler as shown in Fig. S3) and treating variability in tidal conditions (θ) as a uniformly distributed random variable (Eq. 12, Fig. 3). Sediment loads for each day are based on sediment rating curves (Fig. S4), and mean sea level is adjusted based on SLR projections (Fig. S5). The surrogate model was developed to span the range of possible inflows into Newport Bay ($Q = 10$ cms to 1,400 cms), basin elevations ($z_b = 1$ m depth to 6.65 meters depth), and tidal condition θ (peak ebb or peak flood). Note that Fig. 3 only shows the response surface for $Q > 50$ cms for visual clarity. Storms below 50 cms yield complex surfaces due to a higher influence of tidal currents and contribute little to overall basin elevation changes.

The model accounts for dredging policy by testing for the exceedance of the trigger point (2.13 meters below MSL)

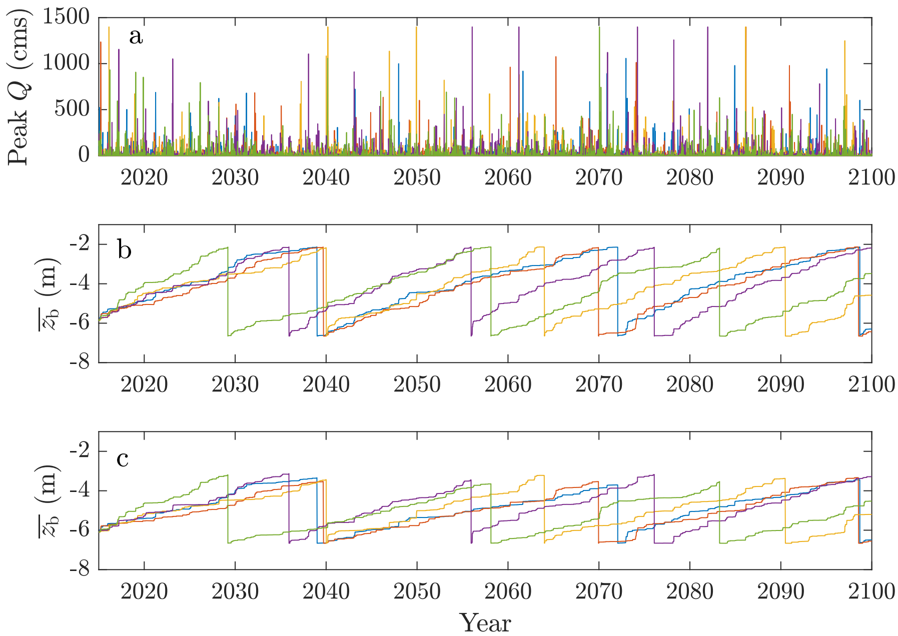

Figure 5: Five examples (color-coded) of multi-decadal MCMC simulations of SDC flow (panel a), Basin I/III elevation (panel b) and Basin II elevation (panel c) using the surrogate model. Dredging events are marked by vertical drop in basin elevation ($\overline{z}_b$), and differences in timing are linked to the occurrence of large storm events (Q). A total of one thousand MCMC simulations are completed to yield probability distributions in expected sedimentation and dredging over future years.

on a daily timescale and resetting the elevation in accordance with the post-dredging elevation. Moreover, various scenarios involving changes in natural forcing and human influences are considered to directly simulate dredging, the decision variable of interest (**D**) as in Figure 1. As an example, Figure 5 shows five MCMC simulations of long-term sediment basin elevation changes for the Unit I/III (b) and Unit II (c) basins given an input of future storm events (a) generated from the MCMC sampler.

Note that sediment basin elevations ($\overline{z_b}$) increase over time, increase in proportion to the occurrence and magnitude of storm events (Q), and are lowered with the occurrence of dredging. Also note significant variability in the timing of dredging which results mainly from the random occurrence of large storm events. Monte Carlo Markov Chain (MCMC) simulations of daily peak Q were used to drive SeAMLESS were run 1,000 times to capture the future uncertainty in dredging scenarios. MCMC transition probabilities were kept constant for the purposes this study, as incorporating climate change is beyond the scope of this work. It is important to note however, that the speed of the surrogate model allows for quick model re-runs and would allow modelers and stakeholders to easily evaluate impacts of changing hydro-climatology on dredging, given a hydrologic model of the watershed.

The timing and occurrence of future dredging events is of interest to stakeholders due to the considerable expense in dredging (roughly \$37 million 2010 dollars per cycle). Fig. 6 demonstrates a potential output of SeAMLESS showing

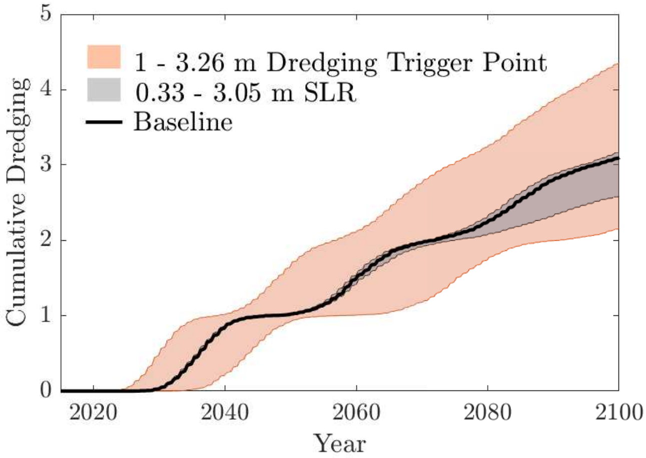

Figure 6: SeAMLESS estimates of the expected number of dredging events through 2100. The baseline scenario (black) corresponds to existing dredging rules and SLR based on the median RCP 4.5 projection (0.61 m by 2100). Colored areas show the range in dredging events based on the range in the dredging trigger point (red) or range in SLR from RCP 2.6 (0.33 m by 2100) and H++ scenario (3.05 m by 2100).

the cumulative likelihood of number of dredging events through 2100 for various scenarios. This was calculated by taking the mean of the MCMC simulations for the cumulative dredging required to maintain minimum basin depth through 2100.

The solid black line shows the cumulative number of required dredging cycles through 2100 under current dredging requirements ($(\overline{z_b})_{\mathrm{trig}}$=-2.13 MSL) and SLR based on the median projection RCP 4.5 scenario (0.61 m by 2100) provided by Griggs et al. (2017). Additionally, the range of dredging cycles corresponding to a range in SLR (through 2100) and a range in the the dredging trigger point are also shown. The low and high levels of SLR are based on RCP 2.6 (0.33 m by 2100) and the H++ scenario (3.05 m by 2100) reported for Southern California by Griggs et al. (2017). High and low value of $(\overline{z_b})_{\mathrm{trig}}$ corresponding to -1.0 m and -3.26 m MSL, or roughly a 1 m change.

Fig. 6 shows that the number of dredging events is not very sensitive to SLR until after 2050, when the differences in SLR become significant. In this limit, the higher SLR scenario (H++) requires less dredging (mean 2.58 total dredging cycles) compared to the minimum SLR scenario (RCP 2.6, mean 3.17 dredging cycles). This trend is a result of SLR adding to basin depth, deepening the basin with respect to the original 2.13 meters below 2015 MSL. Focusing now on the dredging trigger point, what becomes clear is that the effect on the number of dredging cycles is evident within the first two decades of the simulation (before 2040). Additionally, the effect on the total number of dredging cycles is substantial. Maintaining a deeper basin elevation (-3.26 m MSL "trigger point") mandates more than two additional dredging cycles through 2100 based on 4.36 total dredging events for a -3.26 m MSL trigger point and 2.15 dredging events for a -1.0 m MSL trigger point.

The projections shown in Fig. 6 are responsive to the decision-making needs of coastal sediment management stakeholders: probabilities for how much dredging will need to be done, when it needs to be done, and how trigger points (rules) can be adjusted to manage future dredging. As part of the the SedRISE project, an earlier version of this result was presented at a meeting with stakeholders and received favorably. In particular, it was reported that dredging events need to be planned (and budgeted) well over a decade in advance due to challenges with permitting (e.g., Ulibarri et al., 2020), so a multi-decadal forecast of dredging was highly valued. In addition, stakeholders were very interested on how SLR would impact future dredging events. Simple bathtub approaches for investigating the impacts of SLR on coastlines are simple to use and quick to run, but inadequately characterize the dynamic effects of SLR (Passeri et al., 2015). Using SeAMLESS for coastal management is beyond the scope of this paper, but it's important to emphasize that SeAMLESS makes it possible to quickly simulate how a particular management action (in this case dredging) will be affected by environmental factors like SLR and policy factors like dredging trigger points, which is valuable for dialogue and deliberation by stakeholders (DeLorme et al., 2016; Sanders et al., 2020; Stephens et al., 2020).

4. SeAMLESS Application to a Stylized Estuary

A stylized estuary fed by a river and open to the ocean is used to further validate the efficacy of SeAMLESS for predicting average sediment basin elevation over multi-decadal time scales in systems where sedimentation is controlled by loading during storm events, as in southern California. Moreover, we seek to gain a better understanding of SeAMLESS limitations with a second stylized application.

The geometry of the stylized system is presented in Figure 7, and is characterized by a 667 meter wide river from the North at 16 meter depth with respect to mean sea level (MSL). The river opens to a 14×38 km long estuary, with an average depth of 3 meters, and a maintained channel depth of 16 meters. The estuary has a 2×2.5 km sedimentation basin where the river meets the estuary, which is designed to trap riverine material before it enters the lower portions of the estuary, as in Newport Bay. The estuary mouth is 6 km wide with the main channel maintained at 16 meter depth to the open ocean. A high-fidelity Delft3D model is created of this system using a total of 8,993 grid cells, with the highest resolution where the river meets the estuary (100×100 meter spacing) and the coarsest spacing near the oceanic boundaries ($1,000 \times 1,000$ meter spacing).

4.1. High-Fidelity Model

The stylized Delft3D model is forced by streamflow at the northern boundary and a tidal time series at the southern boundary, and all other boundaries were treated as walls. Streamflow was simulated with a 24 hour flood hydrograph, and 12 hour time to rise and fall. The flood peak was randomly generated using Monte-Carlo sampling of peak flows (from 500 - 20,000 cms) which were transformed into daily triangular hydrographs, and sediment load was computed

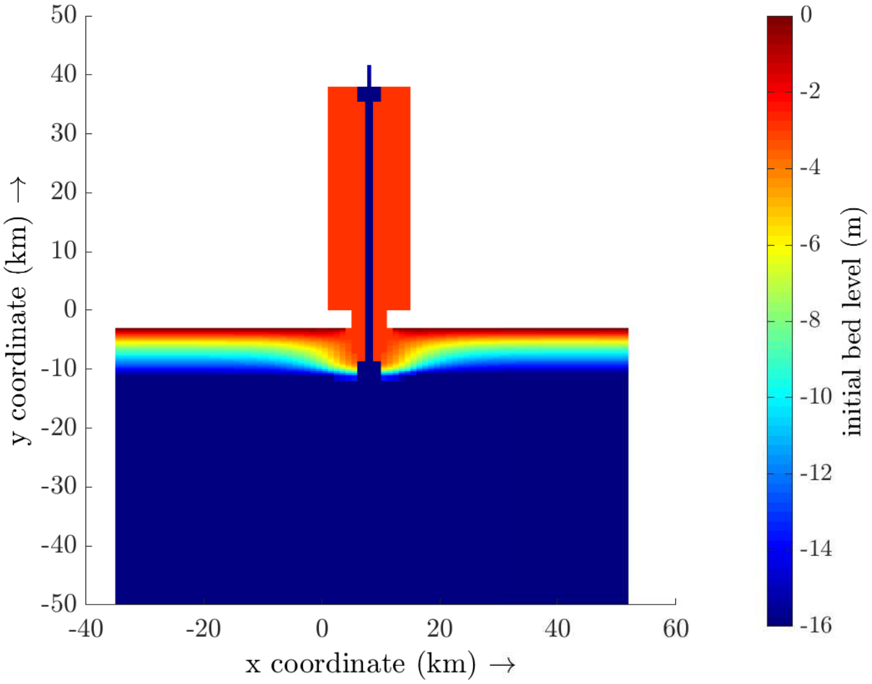

Figure 7: Stylized model model domain and bathymetry.

with an idealized sediment curve. See Fig. S7 for the peak-flow cumulative distribution function and Fig. S8 for sediment-concentration curve used in the high-fidelity stylized model. A period with 500 cms baseflow in the high-fidelity model river lasting a randomly chosen duration between 12-24 hours (uniform distribution) was added between storms to re-establish tidal control of the hydrodynamics and to avoid storm peaks being phase-locked with the tide. Tides were modeled by a 1 meter amplitude tide (with respect to MSL), a period of 12 hours, and phase of zero. Roughness was modeled using the Chezy roughness formula (C=65 m$^{1/2}$/s) with a free slip condition for wall roughness. Two sediment fractions were used, one for sand (dry bed density: ρ_{sand} = 1600 kg/m^3) and mud (dry bed density: ρ_{mud} = 500 kg/m^3, critical bed shear stress for sedimentation and erosion was 1,000 and 0.5 N/m^2, respectively. The initial bed layer was a 5 meter thick bed of sand. The equilibrium condition for sand transport (Van Rijn and Walstra, 2003) was used at the inflow boundary. A morphological scale factor of 5 was used to speed computation with no loss in accuracy (Lesser et al., 2004; Ranasinghe et al., 2011).

4.2. Response Surface Surrogate Model

A response surface surrogate model of the form given by Eq. 12 was developed by running the high-fidelity model for a range of Q and $\overline{z}_b$ values during peak flood and ebb currents and maximum and minimum tides. Peak streamflow values were 500, 1,000, 2,000, 4,000, 6,000, 8,000, 10,000, 15,000, and 20,000 cms. Average sediment basin elevations ranged from a low of 3 meters, up to 16 meters, spaced at intervals between 1 meter (from 3 to 4 meters) to 2 meters of elevation change (from 4 to 16 meters). Sediment yield for the surrogate model was computed for a given peak flow (Q) by integrating the triangular flow hydrograph multiplied by the instantaneous sediment concentration which yielded the regression equation for sediment load shown in Fig. S9. The surrogate model accounted for the morphological scaling factor in the high-fidelity model simulations by multiplying all incoming sediment volumes by the equivalent scaling factor (MF=5). Two variants of the surrogate model were developed based on model simulations which found that $\tilde{\eta}_{\max}$ and $\tilde{\eta}_{\min}$ were coincident with peak flood ($\tilde{\eta}_{flood}(Q, \overline{z}_b)$) and ebb ($\tilde{\eta}_{\mathrm{ebb}}(Q, \overline{z}_b)$) currents as in Newport Bay. However, the authors note that this is site specific, and that high-fidelity model simulations of the system are required to investigate the major controls on $\tilde{\eta}_{\max}$ and $\tilde{\eta}_{\min}$ for each site.

4.3. Multi-Decadal Simulations

Multi-decadal simulation of sedimentation in the stylized estuary was completed by configuring both the high fidelity model and SeAMLESS to depict a sequence of N=200 storm events. In southern California, there are roughly ~5-10 storm events which occur in any given year and thus 200 storms roughly equates to 20-40 years. Integration over events is straightforward using SeAMLESS (Eq. 11). A sequence of 200 consecutive Monte Carlo samples of peak flow created time series of storm events, Q_i, $i = 1, \ldots, N$ which were input into both SeAMLESS and the high fidelity model. These storm peaks were simulated until $Q_i = 200$, or until the basin infilled to 3 meters below mean sea-level, whichever came first. This was repeated for 100 different storm peak sequences (each containing a string of 200 peaks) to sample an exhaustive range of possible storm peak sequences and average out tidal effects. Account of tides between the high fidelity model and SeAMLESS was slightly different in accordance with the functionality of each model: whereas the high-fidelity model uses a random variable to vary the phasing between the storm peak and the tide peak between successive events, SeAMLESS uses a random variable (θ) to compute a weighted average of $\tilde{\eta}_{\max}$ and $\tilde{\eta}_{\min}$. Moreover, for each storm peak sequence, SeAMLESS was repeated 2,000 times using θ as a random variable. Hence, the final sequence of $(\overline{z}_{\mathrm{b}})_i^{\mathrm{SM}}$ for each storm sequence is computed as the average over 2,000 trials and can be considered to be a tidally-averaged solution at the event time scale.

Solutions for each of the 100 different storm sequences were averaged to compute a time series of $(\overline{z}_{\mathrm{b}})_i$ representative of an average over many different possible storm sequences. Hence, the accuracy of SeAMLESS was measured by the mean error (ME) in $\overline{z}_{\mathrm{b}}$ (average over 100 storm sequences) relative to the high-fidelity model (averaged over 100 storm sequences

$$\mathrm{ME} = \frac{1}{N}\sum_{i=1}^{N}(\overline{z}_{\mathrm{b}})_i^{\mathrm{Delft3D}} - (\overline{z}_{\mathrm{b}})_i^{\mathrm{SM}} \tag{13}$$

where N represents the number of events in the storm sequence (when the basin reaches 3 meters below mean sea-level,

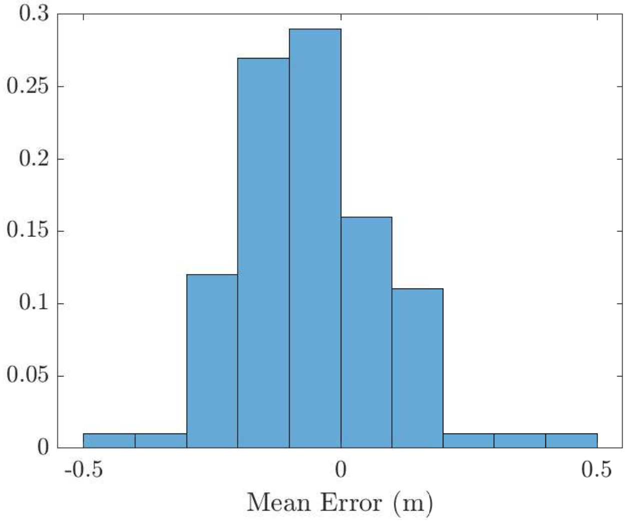

Figure 8: Frequency distribution of Mean Error in $\overline{z}_b$ (Eq. 13) from 100 stochastic storm sequences simulated by SeAMLESS.

or $Q_i = 200$ storm events.

The distribution of errors from 100 different storm sequences is shown in Fig. 8. This distribution passes the K-S test for normality (p=0.47) with a mean of -0.0607 m and standard deviation (σ_{ME}) of 0.1476 m. Conceptually, the results in Fig. 8 indicate that the surrogate model (SM) slightly overestimates average basin elevation by roughly 6 cm on a per-storm basis when compared to the high-fidelity model. This equates to only 0.46% when normalized by overall basin infilling (13 m). Additional insight is obtained by examining the time series predicted by SeAMLESS and the high-fidelity model for specific storm sequences that generate different levels of error, as measured by Eq. 13. Fig. 9 shows time series of $\overline{z}_b$ predicted by SeAMLESS and the high-fidelity model based on ME at a range of quantiles: (a) -95% (b), -5% (c), +5%, and (d) +95%. While the surrogate model tends to underestimate deposition (ME = -0.0607 m), overall, the surrogate model shows nearly equivalent performance compared to Delft3D as the basin is filled. Additionally, the surrogate model performs with roughly an order of magnitude lower ME for the first 100 storm sequences (ME = -0.0061, $\sigma_{\text{ME}} = 0.0922$), indicating that SeAMLESS is especially adept at predicting basin elevation for roughly the first 10-20 years of basin infilling.

We attribute the largest source of error in SeAMLESS simulation to arise from the assumption that sediment bed elevation is uniform across the sedimentation basin, which was used to build the response surface function. Defining T as the time required for the $\overline{z}_b$ to rise up to the top of the sedimentation basin (3 m), Fig. 10 shows contours of bed elevation predicted for t=0, 0.4T, 0.8T, and T. This shows that the sediment basin fills in a non-uniform manner, a feature that is especially evident for $t \geq 0.8T$.

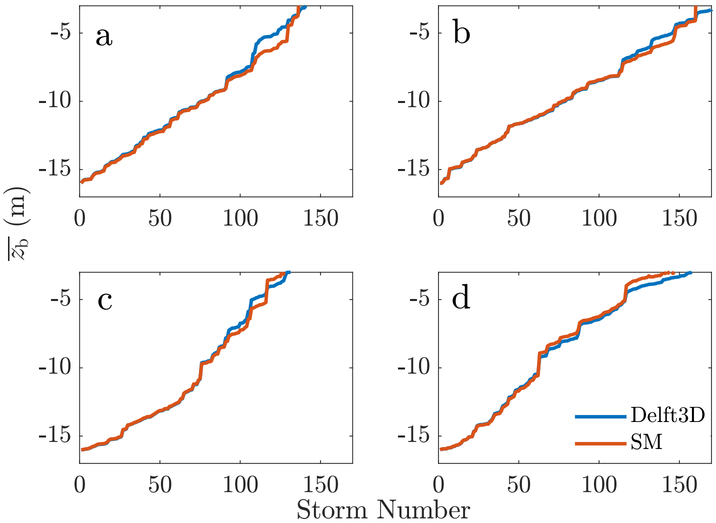

Figure 9: Comparison of high-fidelity model (Delft3D) and SeAMLESS (SM) predictions of $\overline{z}_b$ over 200 sequential storm events for the following quantiles in Mean Error: (a) -95%, (b) -5%, (c) +5%, and d +95%.

5. Conclusions

A reduced-dimension surrogate model for estuarine sedimentation within a managed sediment basin, SeAMLESS, is formulated herein and shown to support multi-decadal simulation with uncertainty and yield decision-variables useful for management in Southern California. Useful output includes the number of expected dredging events in the future, the timing of events, and volumes of sediment associated with these events under different sea level rise scenarios and rules (or “trigger points") for dredging.

SeAMLESS is shown to yield accuracies comparable to a high-fidelity model, while the wall clock run time is reduced by a factor of $\mathcal{O}(10^4)$ even after the high-fidelity model is executed in parallel on a high performance computing cluster with up to 64 cores. The accuracy of SeAMLESS stems from using a calibrated and validated high-fidelity model to develop and parameterize a response surface surrogate model for the capture efficiency of a sedimentation basin, $\tilde{\eta}$, defined as the ratio of sedimentation volume to storm load of sediment over the time scale of a storm event. In essence, SeAMLESS relies on a physics-based model to create a set of data that, in turn, is easily accessed to map out the response of sediment basins to future storm events that bring sediment into the estuary. The computational efficiency of the reduced dimension surrogate modeling approach is shown to support Monte Carlo simulation of future scenarios which provides information about the uncertainty in outcomes.

Sea level rise is expected to reduce the need for dredging in many coastal systems, since high sea levels increase depth. Based on SeAMLESS modeling of Newport Bay, expected dredging through 2100 for the lowest estimate of RCP 2.6 and highest estimate (H++ scenario) sea level rise trajectories reported by (Griggs et al., 2017) corresponded

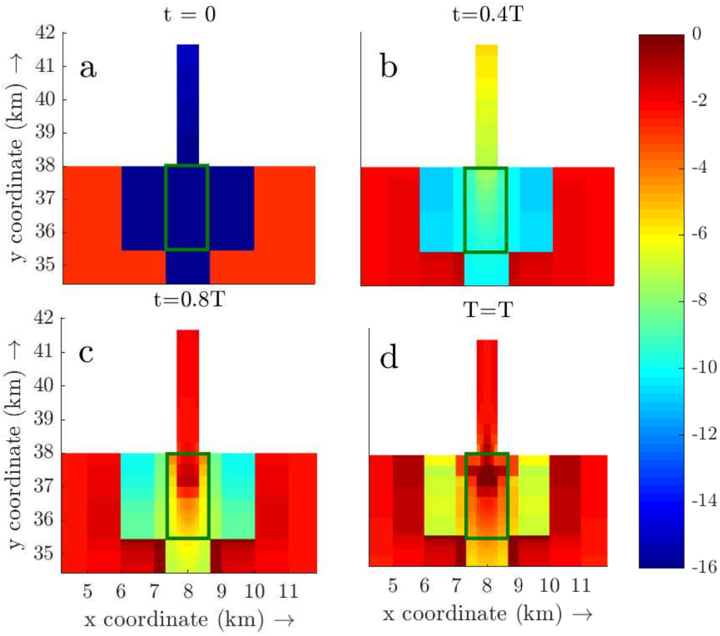

Figure 10: Pattern of sedimentation within the sedimentation basin at times (a) t=0, (b) 0.4T, (c) 0.8T, and (d) T, where T represents the instant the sedimentation basin reaches its capacity and the green rectangle represents the sediment basin definition used to develop the surrogate model.

to 3.2 and 2.6 events, respectively. However, SeAMLESS also shows that moving the trigger height for dredging from 2.13 m (MSL) down to 1 m (MSL) or up to 3.26 m (MSL) could change the expected number of dredging events to 2.1 and 4.4, respectively. This result shows that rules for dredging exert a strong control over the timing and number of dredging events that are needed to manage critical coastal systems like Newport Bay under sea level rise, and reinforce the utility of the SeAMLESS framework as a tool for coastal stakeholder groups to develop rules for dredging under sea level rise.

SeAMLESS was formulated based on coastal embayments in Southern California, where tidal basins are relatively small and experience episodic runoff and sediment loads lasting less than a day, and where dredging is needed to support recreation, navigation, water equality, and ecosystems needs. While this general approach may be appropriate at sites elsewhere, it is important to acknowledge that response surface surrogate models need to be custom built for each site utilizing a high-fidelity numeric model. Hence, a high-fidelity model is important for designing the response surface function (i.e., choice of independent variables) and for parameterizing the response surface function. Based on the results of this paper, the authors conclude that a surrogate model works when deposition is 1) spatially homogenous, 2) the surrogate model area is greater than the numerical model cell size, and 3) confined to a well-defined basin / region. Further research would benefit surrogate model research by investigating developing surrogate models for spatially heterogeneous regions (such as wetlands) using statistical methods to describe the spatial structure of deposition. Additional research incorporating ecological and flood impacts of changing dredging trigger points would improve the utility of the model.

Consideration of a stylized estuary test case also showed that non-uniform filling of the sedimentation basin may emerge as a source of error in the sediment capture efficiency used by reduced-dimension surrogate model. Nevertheless, the accuracy of SeAMLESS was found to be comparable to the high-fidelity model for timescales up to several decades.

6. Acknowledgments

This work is part of the Resilient Infrastructure and Sustainable Environments with Sediment (SedRISE) project funded by an award (#NA16NOS4780206) from the Ecological Effects of Sea Level Rise Program of the National Oceanic and Atmospheric Administration (NOAA), whose support is gratefully acknowledged. We also acknowledge financial support by the Graduate Research Fellowship Program of the National Science Foundation (NSF) for M.W. Brand. The statements, findings, conclusions, and recommendations are those of the author(s) and do not necessarily reflect the views of NOAA or NSF. The authors also acknowledge invaluable input and feedback from the SedRISE Management and Technology Advisory Group (MTAG) and research team, which contributed to the development and application of the SeAMLESS model. In particular, the authors also thank Jian Peng and Jamie Habben at the Orange County Department of Public Works for their support in acquiring data for Newport Bay.

CRediT authorship contribution statement

Matthew W. Brand: Conceptualization of this study, methodology, software, manuscript. **Leicheng Guo:** Methodology, software. **Eric D. Stein:** Revisions to manuscript, overall study guidance. **Brett F. Sanders:** Revisions to manuscript, overall study guidance.

References

Achete, F., Van der Wegen, M., Roelvink, J.A., Jaffe, B., 2017. How can climate change and engineered water conveyance affect sediment dynamics in the san francisco bay-delta system? Climatic change 142, 375–389.

Barbier, E.B., Hacker, S.D., Kennedy, C., Koch, E.W., Stier, A.C., Silliman, B.R., 2011. The value of estuarine and coastal ecosystem services. Ecological monographs 81, 169–193.

Berends, K., Scheel, F., Warmink, J., de Boer, W., Ranasinghe, R., Hulscher, S., 2019. Towards efficient uncertainty quantification with high-resolution morphodynamic models: A multifidelity approach applied to channel sedimentation. Coastal engineering 152, 103520.

Bilskie, M.V., Hagen, S., Alizad, K., Medeiros, S., Passeri, D.L., Needham, H., Cox, A., 2016. Dynamic simulation and numerical analysis of hurricane storm surge under sea level rise with geomorphologic changes along the northern gulf of mexico. Earth's Future 4, 177–193.

Board, C.R.W.Q.C., 2014. Monitoring and reporting for compliance with the total maximum daily load for sediment in the newport bay watershed (santa ana region). URL: http://www.ocwatersheds.com/programs/waterways/tmdl/npbsedimenttmdl.

Bull, L.J., Bull, L.J., Kirkby, M., 2002. Dryland rivers: hydrology and geomorphology of semi-arid channels. John Wiley & Sons.

Chesapeake Bay Program, 2006. Best Management Practices for Sediment Control and Water Clarity Enhancement . Technical Report. URL: https://www.chesapeakebay.net/content/publications/cbp_13369.pdf.

County of Orange, 2013. Newport bay watershed sediment tmdl, 2012-13 annual report. URL: http://www.ocwatersheds.com/programs/waterways/tmdl/npbsedimenttmdl.

County of Orange, 2016. Newport bay watershed sediment tmdl, 2014-15 annual report. URL: http://www.ocwatersheds.com/programs/waterways/tmdl/npbsedimenttmdl.

DeLorme, D.E., Kidwell, D., Hagen, S.C., Stephens, S.H., 2016. Developing and managing transdisciplinary and transformative research on the coastal dynamics of sea level rise: Experiences and lessons learned. Earth's Future 4, 194–209.

Deltares, 2014. Delft3D-FLOW User Manual. volume Version 3.15.

Dewberry, 2013. Coastal California Data Merge Project. Technical Report. National Oceanic and Atmospheric Administration. URL: https://coast.noaa.gov/htdata/lidar1_z/geoid12a/data/2612/supplemental/ca2013_noaa_topobathy_merge_m2612_final_report.pdf.

Elliott, M., Whitfield, A.K., 2011. Challenging paradigms in estuarine ecology and management. Estuarine, Coastal and Shelf Science 94, 306–314.

US Army Corps of Engineers, N., Decision, C.W., Center, S., 2016. The u.s. waterway system: 2015 transportation facts and information. URL: http://www.portsofindiana.com/wp-content/uploads/2017/06/Fact-Card.pdf.

Fedra, K., 1983. Environmental modeling under uncertainty: Monte carlo simulation .

Gallien, T., Schubert, J., Sanders, B., 2011. Predicting tidal flooding of urbanized embayments: A modeling framework and data requirements. Coastal Engineering 58, 567–577.

Griggs, G., Árvai, J., Cayan, D., DeConto, R., Fox, J., Fricker, H., Kopp, R., Tebaldi, C., Whiteman, E., 2017. Rising seas in california: An update on sea-level rise science. California Ocean Science Trust .

Guo, L., Brand, M., Sanders, B.F., Foufoula-Georgiou, E., Stein, E.D., 2018. Tidal asymmetry and residual sediment transport in a short tidal basin under sea level rise. Advances in water resources 121, 1–8.

Haltiner, J., Zedler, J., Boyer, K., Williams, G., Callaway, J., 1996. Influence of physical processes on the design, functioning and evolution of restored tidal wetlands in california (usa). Wetlands ecology and management 4, 73–91.

Isukapalli, S., Roy, A., Georgopoulos, P., 1998. Stochastic response surface methods (srsms) for uncertainty propagation: application to environmental and biological systems. Risk analysis 18, 351–363.

Kiefer, J., Norvell, S., Cohn, E., 2000. The national dredging needs study of ports and harbors-implications to cost-sharing of federal deep draft navigation projects due to changes in the maritime industry (for the us army corps of engineers, institute for water resources).

Kourakos, G., Mantoglou, A., 2009. Pumping optimization of coastal aquifers based on evolutionary algorithms and surrogate modular neural network models. Advances in water resources 32, 507–521.

Koziel, S., Leifsson, L., 2013. Surrogate-based modeling and optimization. Springer.

Kroll, C.G., 1975. Estimate of sediment discharges, Santa Ana River at Santa Ana and Santa Maria River at Guadalupe, California. Technical Report. US Geological Survey.

Lesser, G.R., Roelvink, J.v., Van Kester, J., Stelling, G., 2004. Development and validation of a three-dimensional morphological model. Coastal engineering 51, 883–915.

Liu, J., Dietz, T., Carpenter, S.R., Folke, C., Alberti, M., Redman, C.L., Schneider, S.H., Ostrom, E., Pell, A.N., Lubchenco, J., et al., 2007. Coupled human and natural systems. AMBIO: a journal of the human environment 36, 639–650.

Lotze, H.K., Lenihan, H.S., Bourque, B.J., Bradbury, R.H., Cooke, R.G., Kay, M.C., Kidwell, S.M., Kirby, M.X., Peterson, C.H., Jackson, J.B., 2006. Depletion, degradation, and recovery potential of estuaries and coastal seas. Science 312, 1806–1809.

McLusky, D.S., Elliott, M., 2004. The estuarine ecosystem: ecology, threats and management. OUP Oxford.

Mohammadi, F., Kopmann, R., Guthke, A., Oladyshkin, S., Nowak, W., 2018. Bayesian selection of hydro-morphodynamic models under computational time constraints. Advances in Water Resources 117, 53–64.

Morris, J.T., Barber, D.C., Callaway, J.C., Chambers, R., Hagen, S.C., Hopkinson, C.S., Johnson, B.J., Megonigal, P., Neubauer, S.C., Troxler, T., et al., 2016. Contributions of organic and inorganic matter to sediment volume and accretion in tidal wetlands at steady state. Earth's future 4, 110–121.

Nidzieko, N.J., 2010. Tidal asymmetry in estuaries with mixed semidiurnal/diurnal tides. Journal of Geophysical Research: Oceans 115.

Partheniades, E., 1965. Erosion and deposition of cohesive soils. Journal of the Hydraulics Division 91, 105–139.

Passeri, D.L., Hagen, S.C., Medeiros, S.C., Bilskie, M.V., Alizad, K., Wang, D., 2015. The dynamic effects of sea level rise on low-gradient coastal landscapes: A review. Earth's Future 3, 159–181.

Pritchard, D.W., 1967. What is an estuary: physical viewpoint, American Association for the Advancement of Science.

Ranasinghe, R., Swinkels, C., Luijendijk, A., Roelvink, D., Bosboom, J., Stive, M., Walstra, D., 2011. Morphodynamic upscaling with the morfac approach: Dependencies and sensitivities. Coastal engineering 58, 806–811.

Razavi, S., Tolson, B.A., Burn, D.H., 2012. Review of surrogate modeling in water resources. Water Resources Research 48.

RMA, 1998. Feasibility Report: Upper Newport Bay Numerical Model Development, Baseline Conditions Analysis. Technical Report. US Army Corps of Engineers. URL: `https://www.waterboards.ca.gov/rwqcb8/water_issues/programs/tmdl/docs/Sediment_TMDL/1998_RMA_Model_Baseline_Conditions.pdf`.

Roelvink, J., 2006. Coastal morphodynamic evolution techniques. Coastal engineering 53, 277–287.

Sandbach, S., Nicholas, A., Ashworth, P., Best, J., Keevil, C., Parsons, D., Prokocki, E.W., Simpson, C., 2018. Hydrodynamic modelling of tidal-fluvial flows in a large river estuary. Estuarine, Coastal and Shelf Science 212, 176–188.

Sanders, B.F., Grant, S.B., 2020. Re-envisioning stormwater infrastructure for ultrahazardous flooding. Wiley Interdisciplinary Reviews: Water 7, e1414.

Sanders, B.F., Schubert, J.E., Goodrich, K.A., Houston, D., Feldman, D.L., Basolo, V., Luke, A., Boudreau, D., Karlin, B., Cheung, W., et al., 2020. Collaborative modeling with fine-resolution data enhances flood awareness, minimizes differences in flood perception, and produces actionable flood maps. Earth's Future 8, e2019EF001391.

Schultz, M.T., Small, M.J., Farrow, R.S., Fischbeck, P.S., 2004. State water pollution control policy insights from a reduced-form model. Journal of water resources planning and management 130, 150–159.

Sparrevik, M., Barton, D.N., Bates, M.E., Linkov, I., 2012. Use of stochastic multi-criteria decision analysis to support sustainable management of contaminated sediments. Environmental science & technology 46, 1326–1334.

Sreekanth, J., Datta, B., 2011. Coupled simulation-optimization model for coastal aquifer management using genetic programming-based ensemble surrogate models and multiple-realization optimization. Water Resources Research 47.

Stein, R.G., 2014. Characterizing Dry Weather Runoff, Sediment Resuspension and Associated Bacterial Loads into Newport Bay. Ph.D. thesis. UC Irvine.

Stephens, S.H., DeLorme, D.E., Hagen, S.C., 2020. Coastal stakeholders' perceptions of sea level rise adaptation planning in the northern gulf of mexico. Environmental Management , 1–12.

Thanh, V.Q., Reyns, J., Van, S.P., Anh, D.T., Dang, T.D., Roelvink, D., et al., 2019. Sediment transport and morphodynamical modeling on the estuaries and coastal zone of the vietnamese mekong delta. Continental Shelf Research 186, 64–76.

Thorne, K., MacDonald, G., Guntenspergen, G., Ambrose, R., Buffington, K., Dugger, B., Freeman, C., Janousek, C., Brown, L., Rosencranz, J., et al., 2018. Us pacific coastal wetland resilience and vulnerability to sea-level rise. Science Advances 4, eaao3270.

Trimble, S.W., 1997. Contribution of stream channel erosion to sediment yield from an urbanizing watershed. Science 278, 1442–1444.

Trimble, S.W., 2003. Historical hydrographic and hydrologic changes in the san diego creek watershed, newport bay, california. Journal of historical geography 29, 422–444.

Ulibarri, N., Goodrich, K., Wagle, P., Brand, M.W., Matthew, R., Stein, E., Sanders, B., 2020. Barriers and opportunities for beneficial reuse of sediment to support coastal resilience. Ocean and Coastal Management In Press.

USACOE, 2011. Upper newport bay ecosystem restoration project orange county, california. design documentation report (ddr). URL: https://www.waterboards.ca.gov/rwqcb8/water_issues/programs/tmdl/docs/Sediment_TMDL/2011_ACOE_DDR_Jan2011.pdf.

Van Rijn, L., Walstra, D., 2003. Modelling of sand transport in delft3d-online. Technical Report. Deltares (WL).

Van Rijn, L.C., et al., 1993. Principles of sediment transport in rivers, estuaries and coastal seas. volume 1006. Aqua publications Amsterdam.

Warrick, J.A., Milliman, J.D., 2003. Hyperpycnal sediment discharge from semiarid southern california rivers: Implications for coastal sediment budgets. Geology 31, 781–784.

Yu, Q., Wang, Y., Gao, S., Flemming, B., 2012. Modeling the formation of a sand bar within a large funnel-shaped, tide-dominated estuary: Qiantangjiang estuary, china. Marine Geology 299, 63–76.

MW Brand completed his Ph.D. at the University of California, Irvine.

Highlights

Multi-decadal simulation of estuarine sedimentation under sea level rise with a response-surface surrogate model

Matthew W. Brand,Leicheng Guo,Eric D. Stein,Brett F. Sanders

- Estuarine sedimentation is a complex physical process
- High-fidelity model runtimes hinder multi-decadal simulation
- A response surface surrogate model estimated multi-decadal basin depths
- Surrogate model was orders of magnitude faster compared to high-fidelity model
- Surrogate model was able to attain equivalent accuracy to high fidelity model